Check for updates

ADVANCED FUNCTIONAL MATERIALS
www.afm-journal.de

Protocells Capable of Generating a Cytoskeleton-Like Structure from Intracellular Membrane-Active Artificial Organelles

Dishi Wang, Silvia Moreno, Mengfei Gao, Jiaqi Guo, Bing Xu, Dagmar Voigt, Brigitte Voit, and Dietmar Appelhans**

The intricate nature of eukaryotic cells with intracellular compartments having differences in component concentration and viscosity in their lumen provides (membrane-active) enzymes to trigger time- and concentration-dependent processes in the intra-/extracellular matrix. Herein, membrane-active, enzyme-loaded artificial organelles (AOs) are capitalized upon to develop fluidic and stable proteinaceous membrane-based protocells. AOs in protocells induce the self-assembly of oligopeptides into an artificial cytoskeleton that underlines their influence on the structure and functionality of protocells. A series of microscopical tools is used to validate the intracellular assembly and distribution of cytoskeleton, the changing protocells morphology, and AOs inclusion within cytoskeletal growth. Thus, the dynamics, diffusion, and viscosity of intracellular components in the presence of cytoskeleton are evaluated by fluorescence tools and enzymatic assay. Membrane-active alkaline phosphatase in polymersomes as AOs fulfills the requirements of biomimetic eukaryotic cells to trigger intracellular environment, mobility, viscosity, diffusion, and enzymatic activity itself as well as high mechanical stability and high membrane fluidity of protocells. Thus membrane-active AOs in protocells provide a variable reaction space in a changing intracellular environment and underline their regulatory role in the fabrication of complex protocell architectures and functions. This study contributes significantly to the effective biomimetics of cell-like structures, shapes, and functions.

1. Introduction

The intricate complexity of natural cells is a source of inspiration for researchers in synthetic biology and bioengineering for several decades.[1–5] Due to the immense potential in biomedicine and bioengineering, there is a growing interest in using of biomimetic bottom-up technologies to reconstruct eukaryotic cells with mechanical, morphological, and metabolic features.[4–6] In pursuit of replicating eukaryotic cells in both architecture and functionality, researchers shift their focus from developing structurally simplified assemblies for realizing individual characteristics of cells to search for increasing structural complexity while further diversifying their functions.[1,5–7] Various kinds of cell-like architectures such as polymersomes-in-proteinosome,[8,9] coacervate-in-proteinosome,[10–12] coacervate-in-liposome,[13–15] polymersomes-in-polymersome,[16,17] and liposomes-in-liposome,[18,19] exist to implement the concept of multi-compartmentalization. This endows these protocells with morphology and functionality which can be regulated and modulated to a

D. Wang, S. Moreno, B. Voit, D. Appelhans
Leibniz-Institut für Polymerforschung Dresden e.V.
Hohe Straße 6, D-01069 Dresden, Germany
E-mail: moreno@ipfdd.de; applhans@ipfdd.de

The ORCID identification number(s) for the author(s) of this article can be found under https://doi.org/10.1002/adfm.202306904

© 2023 The Authors. Advanced Functional Materials published by Wiley-VCH GmbH. This is an open access article under the terms of the Creative Commons Attribution-NonCommercial-NoDerivs License, which permits use and distribution in any medium, provided the original work is properly cited, the use is non-commercial and no modifications or adaptations are made.

DOI: 10.1002/adfm.202306904

D. Wang, B. Voit
Organic Chemistry of Polymers
Technische Universität Dresden
D-01062 Dresden, Germany

M. Gao
Max Planck Institute of Molecular Cell Biology and Genetics
Pfotenhauer Straße 108, D-01307 Dresden, Germany

J. Guo, B. Xu
Department of Chemistry
Brandeis University
Watham, MA 02453, USA

D. Voigt
Faculty of Biology
Technische Universität Dresden
D-01062 Dresden, Germany

certain extent, but achieving further progress to mimic a cell's complexity still remains a significant scientific challenge.

The ability to adjust the intracellular environment, to meet physiological and metabolic demands, or to respond to external environmental stimuli, is essential for cells to survive in a dynamic environment. In this regard, the cytoskeleton in cells is characterized by the continuous cytoskeletal assembly/disassembly. It plays a pivotal role to support and enable various cellular dynamic processes such as cell division, intracellular transport, cell migration, and cell signaling.[20–22] Considerable efforts for protocells are directed at reconstructing artificial cytoskeleton to achieve structural and functional regulatory effects similar to their natural counterparts. Current work in this area makes use, for example, of proteinaceous-, amino acid and DNA-based scaffold combined with liposomal and proteinaceous membranes,[9,23,24] or emphasizes the operability of the assembly/disassembly of the proposed synthetic cytoskeleton.[25,26] However, the present efforts still have limitations in providing enhanced mechanical properties of protocells, even though recent achievements are made in liposome-based protocells that regulate cell morphology and internal environment through diverse cytoskeleton assembly.[27–29] In addition, most of the work involving the reconstitution of the artificial cytoskeleton presents only single-compartment platforms such as liposomes,[27–30] proteinosomes,[24] and colloidosomes,[31,32] which may be structurally inadequate to achieve more complex cellular behavior in the future. Thus, it would be highly interesting to validate the formation of cytoskeleton-like structures in multi-compartmentalized protocells (e.g., AOs-based proteinosomes) and their influence on their shape morphology.

To achieve the intracellular formation of cytoskeleton-like scaffolds, the gel-in-vesicle approach is primarily utilized in previous studies.[33–35] Specifically, vesicles are first prepared and gelators are encapsulated within their lumens through post-diffusion or in situ loading, and then external stimuli such as pH,[36] light,[26,37] temperature,[38–40] ion strength,[41] or enzymatic activity[24,31,32,42] are applied to trigger gelation within the vesicles. Among them, the enzyme-induced self-assembly strategy of amino acids/oligopeptides into artificial cellular scaffolds is particularly significant, as it replicates the way, where various biological structures are fabricated through selected assembly processes in cells. Small subunits under the catalysis of specific enzymes can self-assemble into highly ordered and precisely controlled nano-/microstructures via non-covalent interactions.[43,44] This provides a tool to gain deeper insights into the origin of cytoskeletal elements in early cells, which are typically composed of supramolecular combinations of various amino acid derivatives[45] or single nucleotides such as 5′-guanosine monophosphate.[46] Exemplifying this, Mann and coworkers demonstrated the native alkaline phosphatase-(ALP)-induced self-assembly of amino acid-based small hydrophobic molecules, Fmoc- and phosphate-modified tyrosine (Fmoc-TyrP), into the cytoskeleton-like scaffold in protocells.[24,31,32,42] However, due to the limited amphiphilic property of Fmoc-TyrP, the formation condition for artificial cytoskeleton is highly demanding (high concentration of precursors, highly active ALP, and strong alkaline condition). This limits its potential applications under physiological/mild condition. Notably, the oligopeptides designed by Bing and co-workers can undergo dephosphorylation in cells with highly overexpressed ALP and can also concomitantly self-assemble under physiological conditions, without excessive requirements for enzyme activity or oligopeptide concentration.[47–50] Due to their biocompatibility, chemical versatility, and enzymatic biodegradability, these oligopeptides are used in biomedical diagnostics and anticancer therapeutics. Therefore, we consider them highly attractive to be explored for the construction of cytoskeleton-like scaffolds in multi-compartmentalized protocells.

Recently, we developed a novel multi-compartmentalized protocell platform by encapsulating alkaline phosphatase-loaded polymersomes (as AOs or ALP-Psomes) into proteinosomes.[8] The integrated AOs in this biomimetic protocell possess self-reporting characteristics triggered by pH-responsive ALP activity (highest at physiological pH, lower at acidic pH). Due to the insertion of ALP in the membrane of AOs, the enzymatic activity is not controlled by the pH-sensitive swelling of the polymersome membrane. It shows the highest enzymatic activity for dephosphorylation reactions under physiological conditions at which AOs membrane is in the collapsed state. Moreover, the membrane-integrated ALP in AOs offers improved enzyme stability within the biomimetic protocell. It is not released at physiological and acidic pH, but provides a larger contact area of the enzyme with substrate molecules.[8] Thus, ALP in AOs may exhibit similar membrane-active properties as those found in membrane enzyme-rich organelles or at the cell membrane surface in nature.[47–50] Thus, the well-preserved surface reactivity of ALP-Psomes allows for the utilization in enzyme-induced self-assembly strategy when integrated into protocells, enabling the spontaneous assembly of disorderly dispersed subunits into organized intracellular microstructures and cytoskeleton-like scaffolds. Such biomimetic cellular characteristics of ALP-Psomes (**Scheme 1**a) are expected to imitate the occurrence of physiological processes at biological membrane interfaces.

Thus, this work aims to utilize the membrane-integrated and membrane-active ALP in AOs to assemble customizable artificial cytoskeleton within multi-compartmentalized protocells through an enzyme-induced self-assembly strategy (Scheme 1a). This strategy offers the possibility to use time- and oligopeptide concentration-dependent parameters for the regulation of the artificial intracellular environment (=growth of intracellular scaffold in presence of AOs) and to study their influence on the changing protocell´s morphology. To this end, ALP-Psomes as AOs in protocells (ALP-AOPS) are responsible for the dephosphorylation of oligopeptides to induce the self-assembly of even more hydrophobic oligopeptides without phosphate groups into nanofibers up to several microns (Scheme 1b).

Prior to fabricating and characterizing the artificial cytoskeleton in ALP-AOPS, the ALP-Psomes-induced self-assembly of oligopeptides into nanofibers is confirmed using dynamic light scattering (DLS), optical density measurement, atomic force microscopy (AFM), transmission electron microscopy (TEM), and confocal laser scanning microscopy (CLSM) techniques. The same analytical techniques are used for the characterization of multi-compartmentalized protocells, fabricated by the Pickering emulsion process, and of artificial skeleton-containing

© 2023 The Authors. Advanced Functional Materials published by Wiley-VCH GmbH

16163028, 0, Downloaded from https://onlinelibrary.wiley.com/doi/10.1002/adfm.202306904 by Brandeis University, Wiley Online Library on [24/10/2023]. See the Terms and Conditions (https://onlinelibrary.wiley.com/terms-and-conditions) on Wiley Online Library for rules of use; OA articles are governed by the applicable Creative Commons License

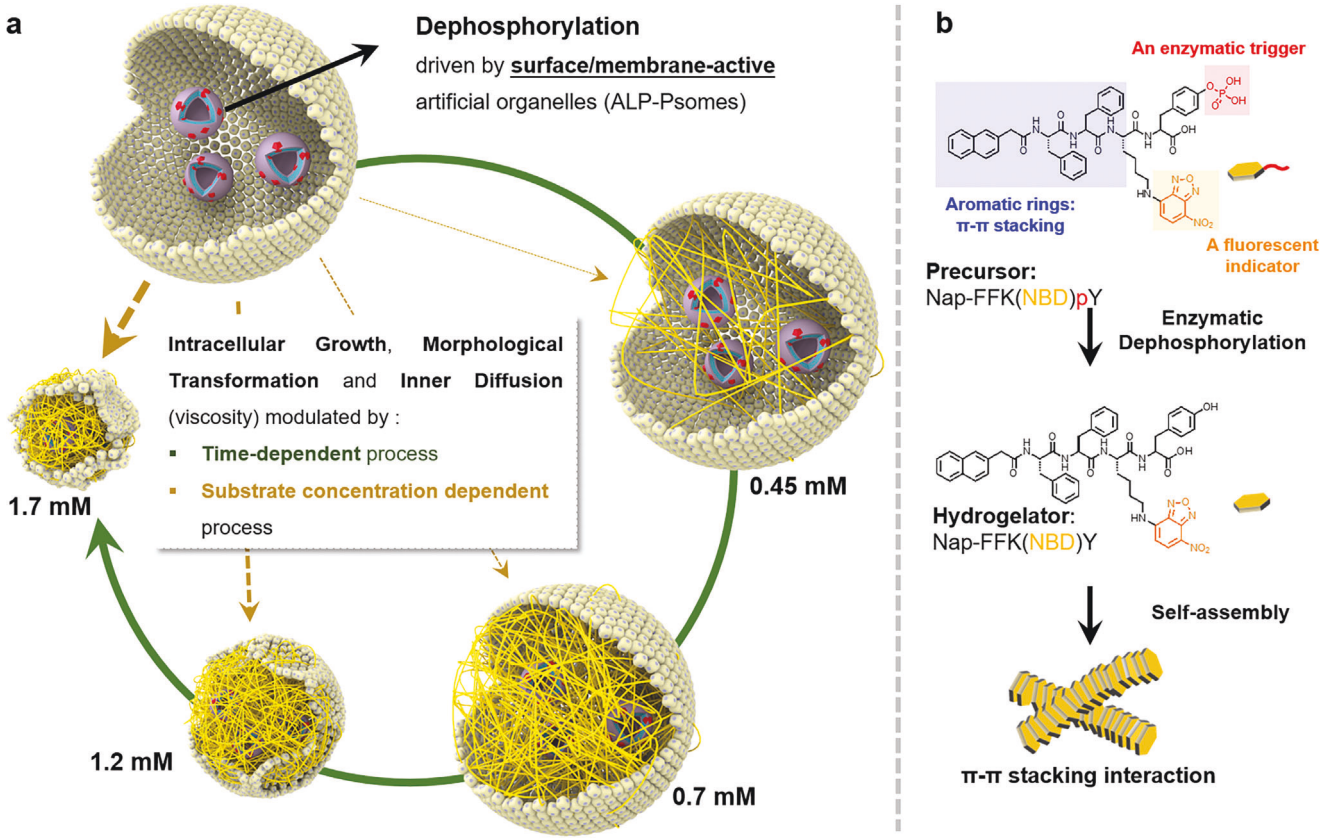

Scheme 1. a) The regulatory role of the artificial cytoskeleton on the morphology of ALP-AOPS protocells during cytoskeletal growth. The intracellular growth is a time- (Green process, 0–3 h) and concentration-dependent process (Yellow, 0–1.7 mM). b) Alkaline phosphatase-instructed dephosphorylation of precursors (Nap-FFK(NBD)pY) to produce hydrogelators (Nap-FFK(NBD)Y) and concomitant nucleation and growth of artificial cytoskeleton via non-covalent interaction.

ALP-AOPS, generated by the post-diffusion of oligopeptides into multi-compartmentalized protocells (Scheme 1a). The morphology and stability of ALP-AOPS with the established intracellular artificial cytoskeleton is additionally supported by cryo-scanning electron microscopy (cryo-SEM). Moreover, the dynamics of intracellular components before and after nanofiber formation in ALP-AOPS are compared using the technology of fluorescence recovery after photobleaching (FRAP). To support the presence of intracellular dynamics in ALP-AOPS, changes in intracellular viscosity along with nanofiber formation are measured by fluorescence anisotropy with respect to the incubation time and oligopeptide concentration. Finally, to validate the effect of intracellular viscosity on the diffusion of substrates, the enzymatic reactivity of ALP in ALP-Psomes integrated in the presence of nanofibers with different densities is compared using fluorescein diphosphate (FDP) as a substrate.

2. Results and Discussion

2.1. Fabrication of Membrane-Active AOs: Proof of Concept of Fiber Growth

As a first step toward cell-like protocells with different shapes (Scheme 1a), artificial membrane-active organelles (membrane-active AOs) based on ALP-Psomes (Figure S4, Supporting Information) are constructed, as reported in our previous work.[8] Briefly, native ALP is added during the self-assembly (in situ) of pH-responsive and photo-cross-linkable amphiphilic block copolymer PEG_{45}-*b*-P(DEAEMA-*s*-DMIBMA)$_{94}$ (Figure S1, Table S1, Supporting Information) into enzyme loaded Psomes (Figure S4, Supporting Information).[51–53] Afterward, the as-formed ALP-Psomes are irradiated by UV light to crosslink the membrane, followed by the purification by hollow fiber filtration (HFF) to remove the unloaded ALP. The loading efficiency (22.21%, 0.044 mg mL^{-1}) is determined using labelled ALP by fluorescence intensity (Figure S5, Supporting Information). Cryo-TEM investigation provides that ALP-Psomes exhibit a similar vesicular structure as found for Empty-Psomes (Figure S6, Supporting Information, further details on diameters and membrane thickness). The pH titration and reversible pH switch studies demonstrate that ALP-Psomes share similar pH-responsiveness and structural robustness as Empty-Psomes in 1 mM PBS (Figure S3a,b, Supporting Information) and the previously reported Enzyme-Psomes.[51,53,54] Moreover, the retention of ALP in Psomes membrane of ALP-Psomes is validated. As expected from the previous study,[8] no significant ALP leakage is observed by a dialysis study at physiological pH (Figure S3c, Supporting Information). Overall, in accordance with our previous study,[8] the ALP-Psomes fabricated here show the expected characteristics and ALP storage over time to provide their

© 2023 The Authors. Advanced Functional Materials published by Wiley-VCH GmbH

16163028, 0, Downloaded from https://onlinelibrary.wiley.com/doi/10.1002/adfm.202306904 by Brandeis University, Wiley Online Library on [24/10/2023]. See the Terms and Conditions (https://onlinelibrary.wiley.com/terms-and-conditions) on Wiley Online Library for rules of use; OA articles are governed by the applicable Creative Commons License

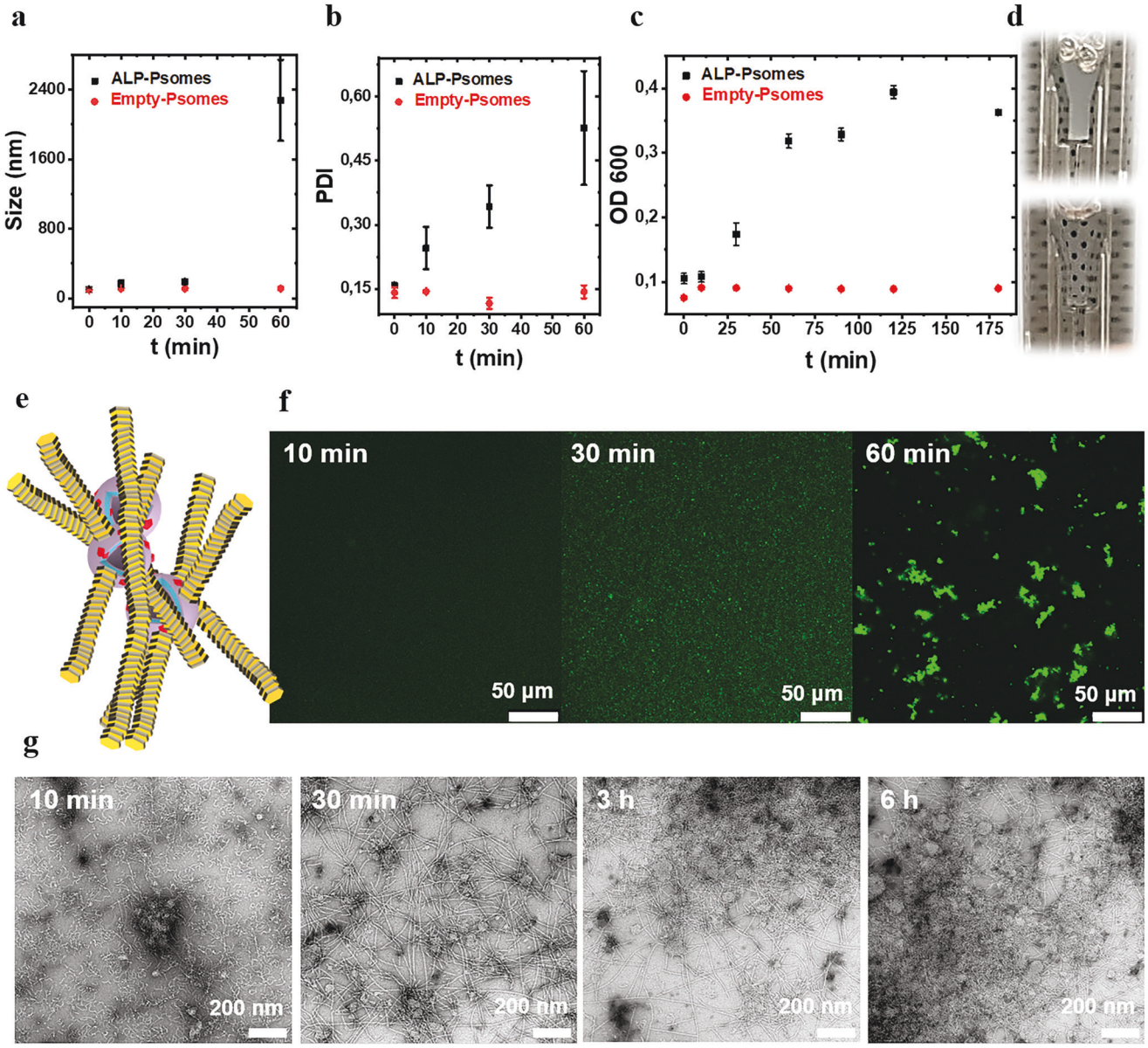

Figure 1. a,b) Characterization of nanofiber triggered by ALP-Psomes in bulk. DLS study on the size distribution of ALP-Psomes and Empty-Psomes in the presence of Nap-FFKpY precursors as a function of time. c) Plots of optical density are shown for ALP-Psomes and Empty-Psomes in the presence of Nap-FFKpY precursors as a function of time. For the studies in (a–c), ALP-Psomes or Empty-Psomes (0.5 mg mL^{-1}) are preincubated with non-labelled 0.7 mM Nap-FFKpY precursors in 10 mM PBS. d) Optical images of Empty-Psomes (bottom) and ALP-Psomes (top) in the presence of 0.7 mM Nap-FFKpY precursors after 3 h incubation. e) Schematic description of the fiber formation instructed by the membrane-active AOs. f) CLSM images of ALP-Psomes in the presence of 0.7 mM Nap-FFK(NBD)pY precursors as a function of time. g) TEM images of ALP-Psomes in the presence of 1.2 mM Nap-FFKpY precursors at selected time points.

surface-activity on demand for the final nanofibers formation in different environments.

Nap-FFK(NBD)pY oligopeptides (with and without fluorescence unit, NBD,) are selected as precursors (Scheme 1b) for the formation of nanofibers in bulk solution (**Figure 1**) and of the artificial cytoskeleton (Figures 3 and 4). Its adaptability for nanofiber formation consists of three key components: i) a well-studied self-assembling backbone (i.e., a diphenylalanine capped with naphthalene (Nap-FF)). The aromatic groups of the L-NAP and L-Phe residue provide sufficient hydrophobic interactions to enable the self-assembly of the dephosphorylated substrate Nap-FFKY to form nanofibers in an aqueous solution; ii) an L-phosphotyrosine (i.e., Yp) to serve as an enzymatic trigger. Nap-FFKpY will be converted to Nap-FFKY after the dephosphorylation by membrane-integrated ALP in ALP-Psomes (Scheme 1a); iii) a fluorescent indicator (i.e., NBD) which will facilitate the fluorescent microscopic investigations. The self-assembly of Nap-FFK(NBD)pY oligopeptides and its analogues into nanofiber/hydrogel, mediated by native ALP in vitro or in vivo, is known.[47,48,50,55] Herein, we use the Nap-FFK(NBD)pY

© 2023 The Authors. Advanced Functional Materials published by Wiley-VCH GmbH

16163028, 0, Downloaded from https://onlinelibrary.wiley.com/doi/10.1002/adfm.202306904 by Brandeis University, Wiley Online Library on [24/10/2023]. See the Terms and Conditions (https://onlinelibrary.wiley.com/terms-and-conditions) on Wiley Online Library for rules of use; OA articles are governed by the applicable Creative Commons License

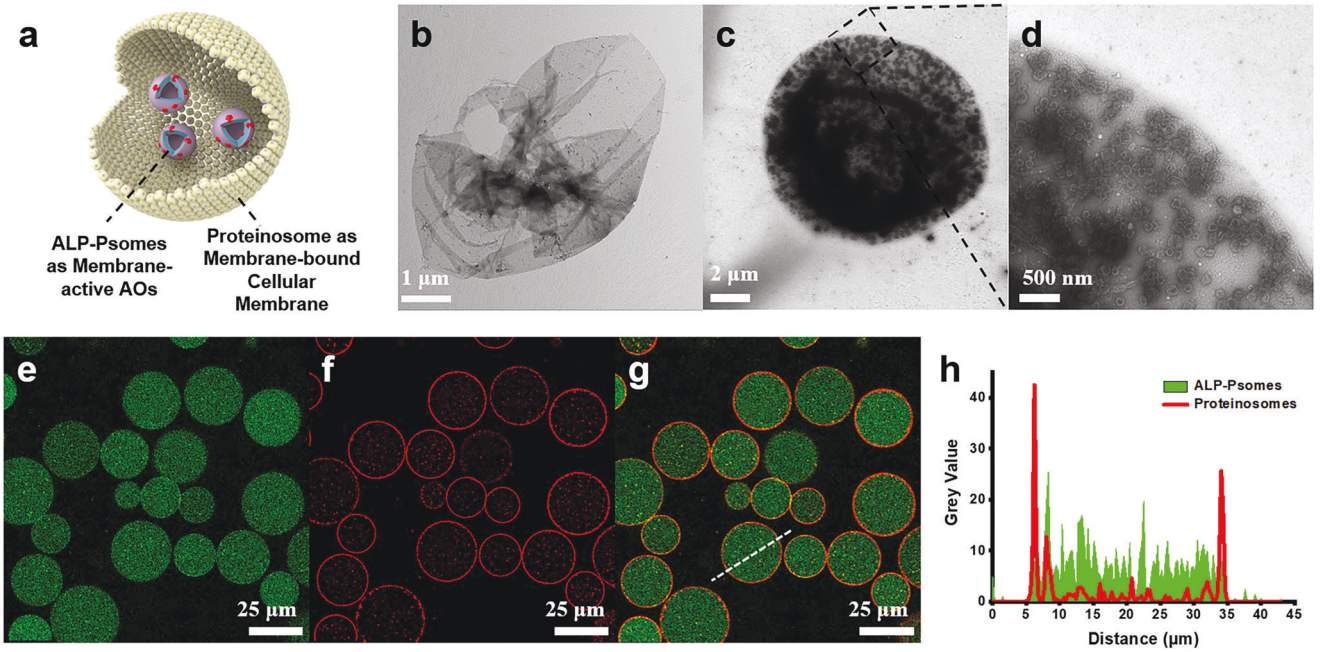

Figure 2. a) Visualization of as-prepared AOPS-ALP microstructures. Schematic describing the architecture of ALP-AOPS with i) ALP-Psomes mimicking AOs and ii) proteinosomes mimicking cellular membranes. TEM images of b) an empty proteinosome and c) an ALP-AOPS structure. d) The magnification image of AOPS presents the intact structure of ALP-Psomes and the partial membrane edge of proteinosome. Both two samples were stained with 2% uranyl acetate. CLSM images of e) AF488-ALP-Psomes, and f) RhB-labelled proteinosomes in aqueous solution. g) Merged image shows the colocalization of ALP-Psomes and BSA-PNIPAAm bioconjugates in ALP-AOPS. h) Corresponding line profile (white dashed line in (g)) of green and red fluorescence intensity across the ALP-AOPS microstructure.

oligopeptide to mimic and reconstruct the artificial cytoskeleton biomimetically by carrying out a local enzymatic reaction from a surface active nano-compartment, ALP-Psomes.

Induced by the dephosphorylation via membrane-active ALP-Psomes, the self-assembly of Nap-FFK(NBD)pY oligopeptides into nanofiber is confirmed by TEM and AFM (Figure S8, Supporting Information). A minimum precursor concentration of 280 μM is required for the nanofiber formation (Figure S9, Supporting Information). Above this concentration long, uniform, and flexible nanofibers (nano is related to the width of the nanofibers) are visualized using TEM, outlining an average width of 7 ± 2 nm and a length of several micrometers. This observation is consistent with previous reports in the literature.[47] The nanofiber formation process is also monitored by DLS and optical density (OD_{600}) using Empty-Psomes as a control. After the addition of precursors, the hydrodynamic diameter of ALP-Psomes slowly increases to several micrometers within 3 h, accompanied by a gradual increase in size distribution. At the same time Empty-Psomes maintain a relatively stable size and size distribution throughout the process (Figure 1a,b; Table S2, Supporting Information). The same conclusion can be made from the turbidity measurements, as the optical density of ALP-Psomes increases significantly over time (Figure 1c,d), while that of the Empty-Psomes remain at their initial level throughout the process. These results indicate that nanofiber growth is a time-dependent process and may lead to the formation of micron-scale aggregated nanofibers induced by ALP-Psomes, also assuming the integration of ALP-Psomes in those formed aggregates in solution.

Subsequently, to gain more insight into the morphology of these aggregates, the growth process is studied at different stages by CLSM (precursor is fluorescently labelled with NBD) and TEM. Along with the enzymatic dephosphorylation, the mixture of ALP-Psomes and precursors become more identifiable, evolving from evenly distributed fluorescence (10 min) to uniformly distributed bright spots (30 min) and eventually to irregularly shaped micro-sized aggregates (1 h) (Figure 1f). In the case of Empty-Psomes no shape-defining objects can be detected during this process (Figure S10, Supporting Information). As shown by TEM images in Figure 1g, initially short worm-like filaments arise (10 min), which turn to be longer filaments after 30 min. At 3 and 6 h, in addition to a denser nanofiber distribution, the clustering between ALP-Psomes and formed nanofibers can also be observed. In the case of Empty-Psomes (Figure S11, Supporting Information), no evidence of nanofiber formation is given throughout the process, except for some adsorption of precursors on ALP-Psomes surface, driven by non-covalent interactions. Overall, we can state that the surface-active characteristic of ALP-Psomes is optimal for initiating the self-assembly of Nap-FFK(NBD)pY oligopeptides into (aggregated) nanofibers.

2.2. Fabrication and Characterization of AOPS with Internal Nanofiber as a Cytoskeleton-Like Scaffold

To establish hierarchically structured protocells (Scheme 1a), proteinosomes are chosen as biomimetic cellular membranes to enclose membrane-active AOs and to serve as hosts to

© 2023 The Authors. Advanced Functional Materials published by Wiley-VCH GmbH

16163028, 0, Downloaded from https://onlinelibrary.wiley.com/doi/10.1002/adfm.202306904 by Brandeis University, Wiley Online Library on [24/10/2023]. See the Terms and Conditions (https://onlinelibrary.wiley.com/terms-and-conditions) on Wiley Online Library for rules of use; OA articles are governed by the applicable Creative Commons License

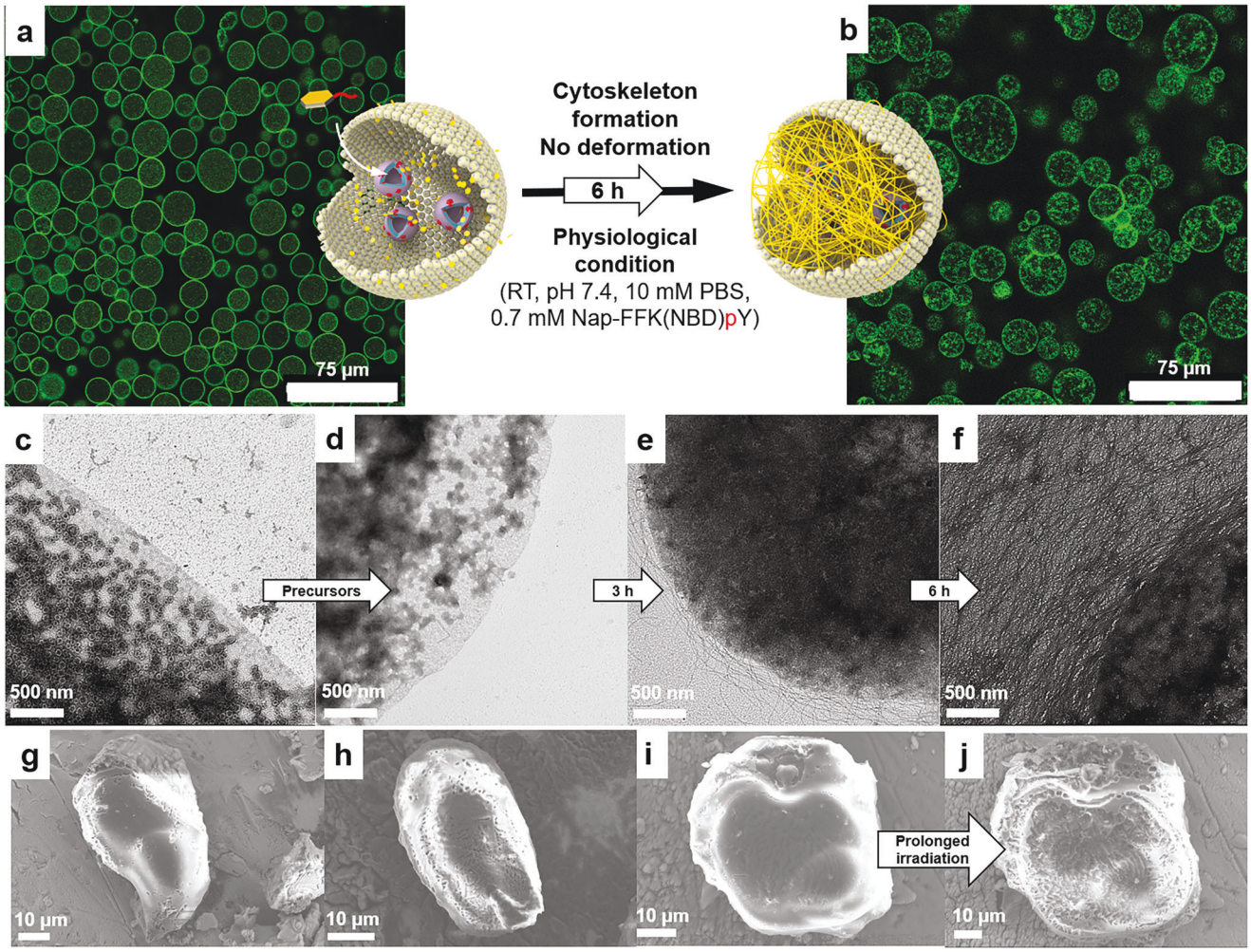

Figure 3. Characterization of AOPS with internal nanofiber as cytoskeleton. a,b) Schematic description of intracellularly cytoskeleton formation triggered by ALP-AOPS. Comparison of CLSM images of ALP-AOPS in the presence of 0.7 mM Nap-FFK(NBD)pY precursors for a) 10 min and b) 6 h. TEM images of ALP-AOPS before the addition of c) 1.2 mM Nap-FFKpY precursors, and d) 30 min, e) 3 h, and f) 6 h after the addition of 1.2 mM precursors. g–i) Cryo-SEM images of ALP-AOPS filled with nanofiber scaffolds, presenting non-spherical protocell morphologies after ≥12 h, as well as j) the image after prolonged electronic irradiation.

accommodate the continuously forming artificial cytoskeleton derived from self-assembled oligopeptides. The selection of proteinosomes is motivated by the following factors: i) the hollow cavity enables efficient encapsulation of a wide range of aqueous nanometer-sized cargoes, including ALP-Psomes, with high loading efficiency;[8,9,52] ii) the covalently crosslinked proteinaceous membrane provides robustness but also flexibility and elasticity due to a well-balanced crosslinking of BSA-PNIPAAm bioconjugates, allowing for the uninterrupted growth of nanofibers within the protocell without the risk of membrane rupture. In contrast, commonly used microscale vesicles such as polymersomes and liposomes suffer from inadequate mechanical properties;[56–58] iii) the semi-permeability of the proteinosome membrane ensures a constant exchange of substances between the interior and exterior of protocells.[8,52,59]

To encapsulate AOs into proteinosomes, ALP-Psomes are mixed with BSA-PNIPAAm bioconjugates in the aqueous solution and then emulsified with the oil phase, generating water-in-oil emulsion (Figure S12, Supporting Information). In this course, BSA-PNIPAAAm bioconjugates with amphiphilic property work as surfactants to stabilize the resulting emulsion at the interface, while ALP-Psomes are partitioned within the aqueous droplet. After membrane crosslinking and phase transfer, ALP-Psomes-containing proteinosomes (ALP-AOPS) are obtained (**Figure 2**a).[8] The encapsulation of ALP-Psomes by proteinosomes is verified by TEM study. In comparison to empty proteinosomes with their rather transparent proteinaceous membrane (Figure 2b), polymersome-like particles can be clearly visualized within the lumen of ALP-AOPS. This observation indicates that the encapsulated ALP-Psomes remain structurally intact after encapsulation (Figure 2c,d). The structural composition of the resulting ALP-AOPS is further confirmed by CLSM study (Figure 2e–h). To visualize each building blocks in ALP-AOPS, ALP, and BSA-PNIPAAm bioconjugates are fluorescently labelled with AF488 and rhodamine B (RhB), respectively. The electrostatic repulsion between ALP-Psomes and BSA-PNIPAAm

© 2023 The Authors. Advanced Functional Materials published by Wiley-VCH GmbH

16163028, 0, Downloaded from https://onlinelibrary.wiley.com/doi/10.1002/adfm.202306904 by Brandeis University, Wiley Online Library on [24/10/2023]. See the Terms and Conditions (https://onlinelibrary.wiley.com/terms-and-conditions) on Wiley Online Library for rules of use; OA articles are governed by the applicable Creative Commons License

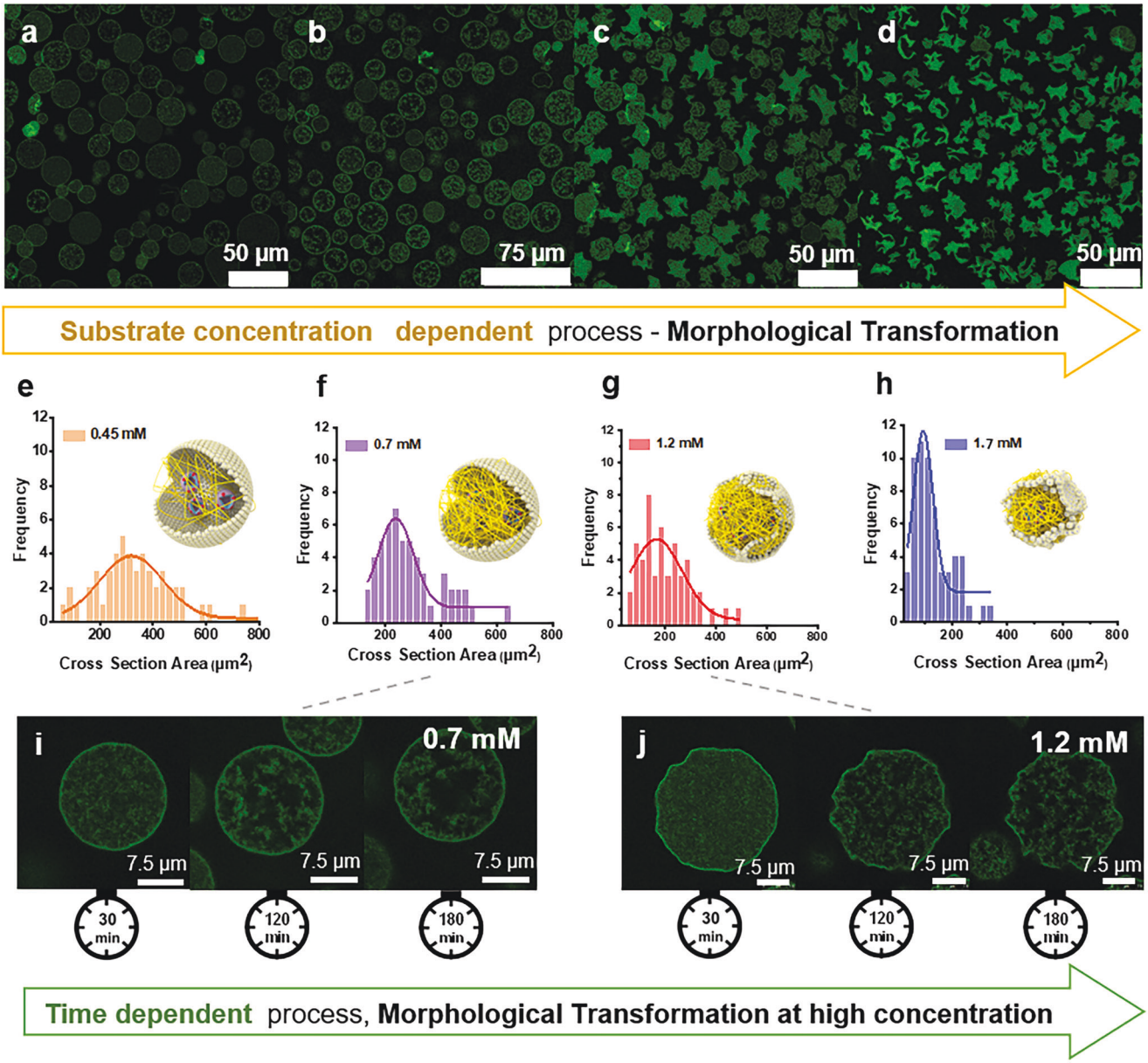

Figure 4. Study of intracellular growth process and morphological transformation. a–d) CLSM images, and e–h) statistical distribution of sectional area of ALP-AOPS after the incubation with Nap-FFK(NBD)pY precursors at concentrations of a,e) 0.45 mM, b,f) 0.7 mM, c,g) 1.2 mM, and d,h) 1.7 mM for 3 h in 10 mM PBS. Statistical distributions of sectional area of ALP-AOPS are calculated from fluorescence microscopy images by manually analyzing 50 proteinosome particles via ImageJ. Average grey value per ALP-AOPS is calculated from fluorescence microscopy images by manually analyzing 50 proteinosome particles via ImageJ. Time-dependent confocal microscopy showing in situ growth of the Nap-FFK(NBD)pY nanofiber within a single ALP-AOPS produced by addition of Nap-FFK(NBD)pY at i) 0.7 mM and j) 1.2 mM to the external phase of a dispersion of ALP-AOPS. j) Note the large degree of microcapsule shrinkage accompanying the gelation process. Note: the full-time CLSM observation of ALP-AOPS in the presence of Nap-FFK(NBD)pY (0.7 and 1.2 mM) is presented in Figure S19, Supporting Information.

preferentially leads to a distinct separation in their respective locations (Figure S7, Supporting Information), as evidenced by the line profile of Figure 2h. Considering the uniform green and red fluorescence throughout the interior of AOPS, this suggests that ALP-Psomes are homogeneously distributed in the lumen of AOPS. In opposite, most of RhB-labelled BSA-PNIPAAm bioconjugates are assembled into the outer membrane of AOPS. Taken together, multi-compartmentalized protocells with a semipermeable crosslinked membrane and loaded with membrane-active AOs are successfully constructed and are ready for the next steps in our study.

Using the permeability of ALP-AOPS membrane for capturing cargo below 40 kDa, we apply a post-loading strategy of oligopeptide precursors to let diffuse them inside of ALP-AOPS and then to immediately start their self-assembly into nanofibers in a defined confinement (Scheme 1a).[8,9,59] Theoretically, the added

© 2023 The Authors. Advanced Functional Materials published by Wiley-VCH GmbH

16163028, 0, Downloaded from https://onlinelibrary.wiley.com/doi/10.1002/adfm.202306904 by Brandeis University, Wiley Online Library on [24/10/2023]. See the Terms and Conditions (https://onlinelibrary.wiley.com/terms-and-conditions) on Wiley Online Library for rules of use; OA articles are governed by the applicable Creative Commons License

precursor will diffuse through the ALP-AOPS membrane, undergo dephosphorylated, and concomitantly self-assemble into nanofibers. This process is illustrated in **Figure 3**a,b, initially validated through CLSM study, with ALP-Psomes homogeneously distributed within the lumen of ALP-AOPS (Figure 2h). Following treatment with ALP-AOPS after 10 min, the precursors (shown by the green fluorescence) are uniformly dispersed within the lumen of the proteinosomes, but in addition preferentially adsorbed onto the proteinosome membrane (Figure 3a). This effect is possibly caused by the electrostatic attraction between the negatively charged precursors and positively charged BSA-PNIPAAm and ALP-Psomes (Figure S7, Supporting Information). It is assumed that the proteinaceous membrane of ALP-AOPS acts as a diffusion barrier to slowly release the precursor to cationic ALP-Psomes in the lumen of ALP-AOPS. After 6 h of incubation, the fluorescence distribution of dephosphorylated oligopeptide-based nanofibers in AOPS becomes heterogeneous (Figure 3b). This heterogenization implies a preferred clustering between ALP-Psomes and nanofibers inside ALP-AOPS, similar to the previous study in bulk solution (Figure 1d). It cannot be excluded that there are also interacting nanofibers along the cationic proteinaceous membrane of ALP-AOPS after 6 h.

To further verify this observation, TEM is undertaken to visualize the ALP-AOPS at specific time points. Prior to the addition of Nap-FFK(NBD)pY precursors, imaging of ALP-AOPS displays the highly electron-transparent proteinosome membrane edge along with integrated ALP-Psomes (Figure 3c; Figure S13, Supporting Information). After 30 min of adding Nap-FFK(NBD)pY precursors, the structural features of ALP-Psomes become blurred, and ALP-AOPS still exhibit a partially electron-transparent proteinosome membrane without any nanofibers formed on the external surface of ALP-AOPS. This development indicates that the formation of nanofibers may remain preferentially confined to the interior of ALP-AOPS at this stage (Figure 3d). At the 3 h time point, nanofibers growth starts from the inner lumen of ALP-AOPS and extends to the outside of ALP-AOPS membrane. Additionally, ALP-AOPS exhibit an electron-dense microsphere, which is associated with the increasing density of nanofibers growing in the inner lumen of proteinosomes (Figure 3e). After 6 h, the lumen of proteinosomes is typically packed with nanofibers (Figure 3f). However, the diffusion of a large excess of Nap-FFK(NBD)pY precursors from the external phase into the lumen of proteinosomes is still possible; these oligopeptides will be dephosphorylated by ALP-AOPS, and further assembled. This process explains the further outgrowths of nanofibers through a still permeable ALP-AOPS membrane after 6 h (Figure 3f). In contrast, no fibers formation is observed throughout the process after adding Nap-FFK(NBD)pY precursors to empty AOPS due to the absence of ALP enzyme in Psomes (Figure S14, Supporting Information). Overall, the TEM investigation verifies the growth process of nanofiber assembling within AOPS and their gradual extent to the outside ALP-AOPS membrane.

Finally, cryo-SEM allows further insights into the structural features of ALP-AOPS with embedded (aggregated) nanofibers in their lumen. Due to the instability of water-rich containing system under cryo-SEM conditions (e.g., prolonged electron beam), it is not possible to verify intact proteinosome structures for ALP-AOPS without oligopeptides, where no cytoskeleton-like scaffold can be formed within the proteinosome. The ALP-AOPS outer membrane immediately collapses and disintegrates (Figure S15, Supporting Information). This alteration is consistent with our previous cryo-SEM investigation.[52] However, due to a stabilizing effect of the formed nanofibers in ALP-AOPS in the presence of oligopeptides (after incubation for 12 h), intact ALP-AOPS can be verified (Figure 3g–i; Figure S16, Supporting Information). The ALP-AOPS do not show a perfect spherical structure, for example, as observed by CLSM, Figure 3a,b) but other non-spherical protocell morphologies. These shapes can be a result of rigid scaffold formation. The well-preserved structural integrity of the single ALP-AOPS architecture demonstrates that the nanofiber-based scaffold with cytoskeleton-like characteristics effectively enhances the mechanical properties of ALP-AOPS with a proteinaceous membrane. We can further observe that the membrane of ALP-AOPS is only slightly disrupted even after prolonged electron beam during cryo-SEM investigation, showing some hydrogel-like porous areas of the ALP-AOPS membrane (Figure 3i,j; Figure S16a,b, Supporting Information). This appearance implies a significantly higher stability of ALP-AOPS after prolonged electron beam for the enlargement of ALP-AOPS membrane compared to ALP-AOPS membrane. A closer examination of the ALP-AOPS membrane confirms the presence of a porous cytoskeleton-like scaffold widely distributed throughout the lumen of ALP-AOPS after prolonged electron beam (Figure S16c, Supporting Information). We assume that the fibrillar microstructures originated from the inner lumen stabilize the outer membrane of ALP-AOPS also under prolonged electron beam. Overall, it can be stated that the self-assembly of precursors into artificial cytoskeleton is well available and highly reproducible, using the enzymatic activity of membrane-active AOs, and leads to a significantly more mechanically stable protocell structure.

2.3. Intracellular Growth of Artificial Cytoskeleton and Morphological Transformation of Protocells: Concentration- and Time-Dependent Process

Concluding previous results (Section 2.2), intracellular construction of artificial cytoskeleton can be initiated by our membrane-active AOs in ALP-AOPS (Scheme 1a). Next, a notable and beneficial characteristic of the cytoskeleton is its capacity to regulate cellular physiological activities by modulating the intracellular environment. This feature is often attributed to different states of the crowdedness of intracellular components, also visible by a change in the intracellular viscosity, reorganization, and partial morphological alteration of cells. Concentration- and time-dependent parameters are applied to investigate the regulatory role of the artificial cytoskeleton on our protocells.

Thus, ALP-AOPS are preincubated with various precursor concentrations. The CLSM investigation reveals that ALP-AOPS maintain a spherical shape when incubating them with precursors at relatively low concentrations (0.45 and 0.7 mM) (**Figure 4**a,b; Figure S17a,b, Supporting Information). After 3 h AOs-mediated nanofiber growth, intracellular fluorescence becomes progressively heterogeneous (Figure 4i; Figure S18a, Supporting Information). Interestingly, as the precursor concentration is increased to 1.2 mM, besides heterogeneously increasing fluorescence

© 2023 The Authors. Advanced Functional Materials published by Wiley-VCH GmbH

16163028, 0, Downloaded from https://onlinelibrary.wiley.com/doi/10.1002/adfm.202306904 by Brandeis University, Wiley Online Library on [24/10/2023]. See the Terms and Conditions (https://onlinelibrary.wiley.com/terms-and-conditions) on Wiley Online Library for rules of use; OA articles are governed by the applicable Creative Commons License

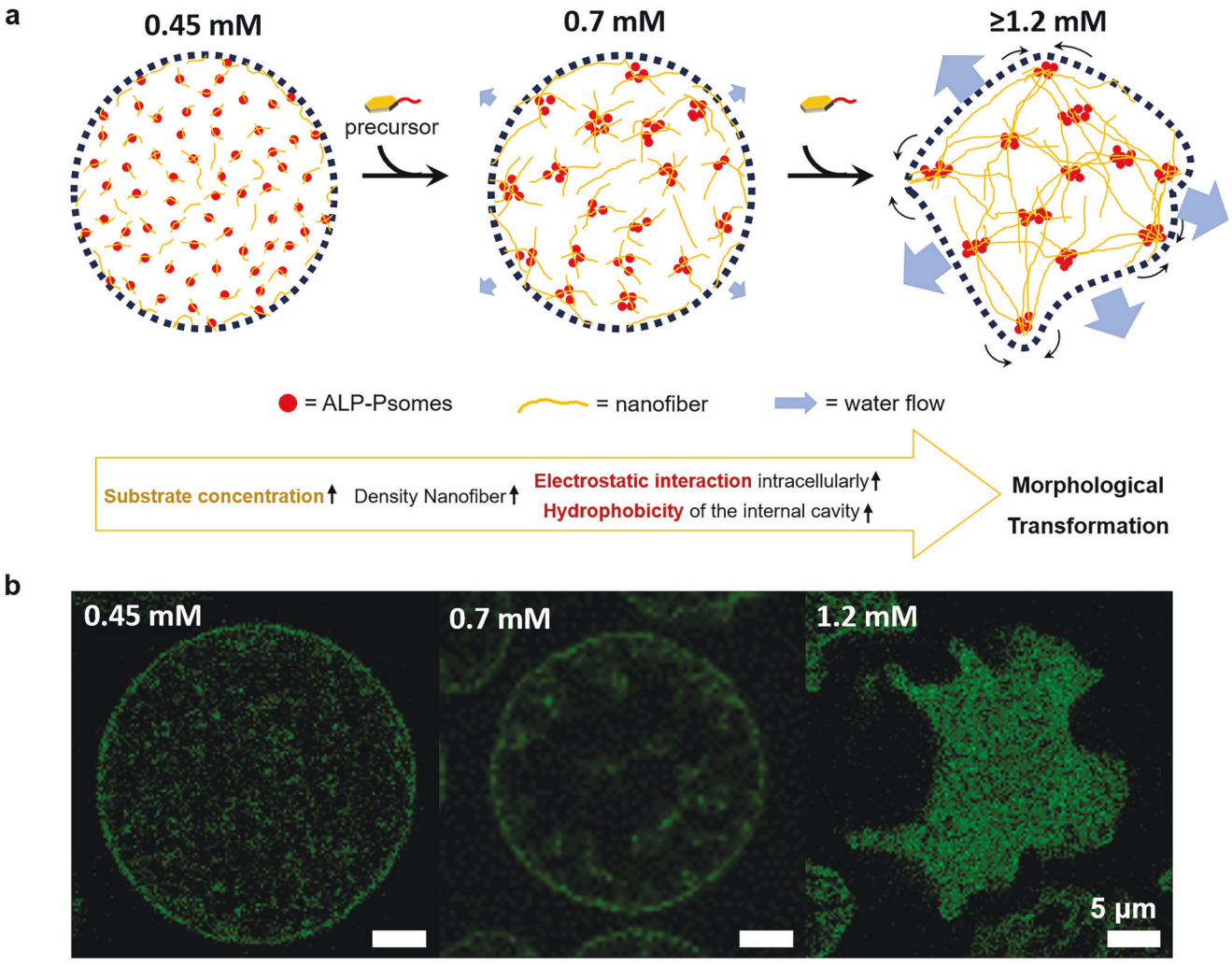

Figure 5. Simplified mechanism on the assembled nanofibers in the presence of AOs, ALP-Psomes, through the concentration-dependent process. Morphological transformation, at 3 h incubation time for each concentration, from spherical-like shapes (0.45 and 0.7 mM) into irregular shapes (≥1.2 mM), triggered by non-covalent interactions (ionic and hydrophobic) between the cationic proteinaceous membrane and ALP-Psomes and (anionic) hydrophobic nanofibers. a) Water repulsion can be also assumed from inside to outside. b) Selected CLSM images of individual protocells at various concentrations after 3 h incubation of precursor.

distribution, ALP-AOPS undergo unexpected morphological transformation processes (e.g., a kind of shrinkage), becoming non-spherical and of irregular shapes (Figure 4c,j; Figures S17c,S18b, Supporting Information). The morphological transformation processes become even more pronounced, when the concentration is further increased to 1.7 mM (Figure 4d; Figure S17d, Supporting Information). To elucidate this phenomenon, statistical analysis of the sectional area of individual ALP-AOPS (Figure 4e–h) suggests that the maximal statistical area of ALP-AOPS is in the range between 90 and 300 μm^2 by varying the concentration of precursors for nanofiber formation. Additionally, the density of the nanofibers assembled in the ALP-AOPS lumen increases with the incubated precursors concentration (Figure S19, Supporting Information). However, the control experiments involving the incubation of empty AOPS with precursors (at concentrations of 0.7 and 1.2 mM) do not show significant alterations in fluorescence distribution or volume contraction, regardless of the durations of incubation or the concentration of the precursors (Figure S20, Supporting Information). We attribute this intracellular reorganization and morphological transformation processes (=deformation processes of "spherically shaped ALP-AOPS") to the electrostatic interaction of negatively charged nanofibers with the rest of the positively charged intracellular components (Figure S7, Supporting Information). In addition, the increasing hydrophobicity of the internal cavity can be another potential driving force previously reported.[47,60] **Figure 5** briefly summarizes a simplified mechanisms for cytoskeleton-like scaffold formation and morphological transformation processes, also known from liposomal systems.[27–29] Driven by the continuous process of dephosphorylation and subsequent self-assembly, the precursors are condensed and concomitantly assembled into nanofibers within the ALP-AOPS. Initially, the growing nanofibers trigger intracellular clustering with

© 2023 The Authors. Advanced Functional Materials published by Wiley-VCH GmbH

16163028, 0, Downloaded from https://onlinelibrary.wiley.com/doi/10.1002/adfm.202306904 by Brandeis University, Wiley Online Library on [24/10/2023]. See the Terms and Conditions (https://onlinelibrary.wiley.com/terms-and-conditions) on Wiley Online Library for rules of use; OA articles are governed by the applicable Creative Commons License

ALP-Psomes. As the concentration of the negatively charged precursor in contact with ALP-AOPS increases, the continuously growing nanofibers further interact with cationic proteinosome membranes through electrostatic interactions, leading to their inward contraction. Meanwhile, evolving nanofibers might also provide a progressively enhanced local hydrophobic environment, promoting the expulsion of water and, thus, trigger the collapse of proteinosome morphology.[47,60] Although it is still tricky to figure out which factor is dominating, it can be concluded that ALP-AOPS in the presence of a higher concentration of precursors can fabricate an increasing nanofiber-based scaffold density in the cavity of ALP-AOPS.

Finally, this results in a larger volume contraction and also confirms the validated mechanical stability of artificial cytoskeleton-based ALP-AOPS under cryo-SEM conditions. This reinforcement also implies that postulated interactions of fibrillar microstructures of assembled oligopeptides and proteinaceous membrane of ALP-AOPS exist (Figure 3g–j). Overall, this also shows us that the proteinaceous membrane of ALP-AOPS outlines a high robustness and high state of elasticity due to the presence of crosslinked proteinaceous membrane of ALP-AOPS.

2.4. Dynamics and Viscosity of Artificial Skeleton-Based ALP-AOPS and Their Influence on ALP Activity

The final consideration is directed to validate the dynamics of ALP-Psomes as AOs and their enzymatic activity under the established nanofiber-based cytoskeleton-like scaffold in the protocells of ALP-AOPS.

Therefore, there is a need to study the dynamics of nanofiber-based scaffold in ALP-AOPS. For that, FRAP is undertaken by photobleaching a small fluorescent region within ALP-AOPS.[15,61] Empty AOPS pretreated with precursors are also used as a control. FRAP measurements are carried out after 6 h incubation for both protocell systems, using 0.7 mM precursor. Following local photobleaching, a gradual recovery of fluorescence up to 75% of the original value within 2 min can be observed in empty AOPS (**Figure 6**a, bottom; Figure 6b). This finding indicates that the mixture of Empty-Psomes and precursors still possesses a certain degree of dynamics and mobility within the AOPS. In contrast, the bleached region of fluorescent aggregated nanofibers with AOs in ALP-AOPS exhibits no significant fluorescence recovery within the same time frame (Figure 6a, top; Figure 6b). The mobility fraction of nanofiber-filled ALP-AOPS is 0.06, which is considerably lower than that of the control (0.76) (Figure S21, Supporting Information). This result indicates that the enzymatic dephosphorylation of the precursor by ALP-Psomes and subsequent spontaneous self-assembly of the nanofibers result in the formation of a relatively rigid intracellular scaffold with low dynamics. The rigidity of nanofibers/ALP-Psomes-based scaffold formed within ALP-AOPS also leads to the enhanced mechanical stability of ALP-AOPS (membrane), as discussed for the cryo-SEM results (Figure 3g–j).

To gain a deeper understanding of the effects of nanofiber growth on the fluidity and viscosity of the intracellular microenvironment, the motility of intracellular components in ALP-AOPS is determined by measuring fluorescence anisotropy of integrated ALP-Psomes (Figure S22, Supporting Information). To this end, RhB-labelled block copolymers are synthesized for the fabrication of ALP-Psomes-RhB (Figures S2 and S4, Table S1, Supporting Information), while both ALP and precursors used in this study are non-fluorescently labelled. Subsequently, to monitor changes in intracellular viscosity resulting from nanofiber formation, different concentrations of non-labeled precursors in ALP-AOPS-RhB are used to evaluate the fluorescence anisotropy at specific time intervals, using empty AOPS-RhB as a control. Based on the positive correlation between fluorescence anisotropy and viscosity (Figure S23, Supporting Information), the local viscosity in ALP-AOPS is potentially controllable through the degree of precursor addition. This correlation is confirmed by the precursor concentration-dependent fluorescence anisotropy of ALP-AOPS-RhB. Thus, higher precursor concentrations result in elevated levels of fluorescence anisotropy as proven for ALP-AOPS-RhB after 3 h of incubation (Figure 6C). In contrast, empty AOPS-RhB exhibit no significant changes in fluorescence anisotropy with respect to the precursor concentration or incubation time (Figure 6C). Overall, we can state that the viscosity of the internal environment is adjustable through the self-assembly of oligopeptides into nanofibers-based scaffold in protocells, induced by ALP Psomes. Such manipulation of the intracellular microenvironment allows for modulating the activity of embedded enzymes in the protocells of ALP-AOPS.

To assess this potential enzyme modulation, the enzymatic reactivity of ALP-Psomes is examined by utilizing small molecule non-fluorescent FDP as a substrate and its quantified dephosphorylation to a fluorescent product, fluorescein (Details in Supporting Information). In the presence of a nanofiber-based scaffold in ALP-AOPS, the enzymatic activities at different pH values are compared, indicating that the pH-responsive nature of ALP can be preserved effectively. This preservation implies that the ALP characteristics in the protocells are not suppressed in the presence of a nanofiber-based scaffold (Figure S24, Supporting Information). Moreover, ALP-AOPS with embedded 0.7 mM nanofibers-based scaffold exhibit a relatively lower activity than that of water-filled ALP-AOPS. This lower activity is obviously attributed to the kinetic limitations arising from the reduced diffusion rate of the substrate through the viscous supramolecular scaffold (Figure 6D). Such a reduction in enzymatic dephosphorylation is more pronounced in ALP-AOPS containing 1.7 mM nanofibers-based scaffold, showing a threefold decrease compared to water-filled ALP-AOPS. This result is in good agreement with the concentration-dependent viscosity modulation of the intracellular environment revealed by the fluorescence anisotropy study.

3. Conclusions

In conclusion, ALP-Psomes-based AOs successfully outline the expected membrane-active characteristics as known from cells to carry out dephosphorylation reactions in different intracellular environments. Due to enzymatic dephosphorylation reactions, these AOs possess the capability to induce the self-assembly of oligopeptides into nanofibers via non-covalent interactions. Such membrane-driven dephosphorylation of AOs is still effective for the formation of a fibrillary artificial cytoskeleton within

© 2023 The Authors. Advanced Functional Materials published by Wiley-VCH GmbH

16163028, 0, Downloaded from https://onlinelibrary.wiley.com/doi/10.1002/adfm.202306904 by Brandeis University, Wiley Online Library on [24/10/2023]. See the Terms and Conditions (https://onlinelibrary.wiley.com/terms-and-conditions) on Wiley Online Library for rules of use; OA articles are governed by the applicable Creative Commons License

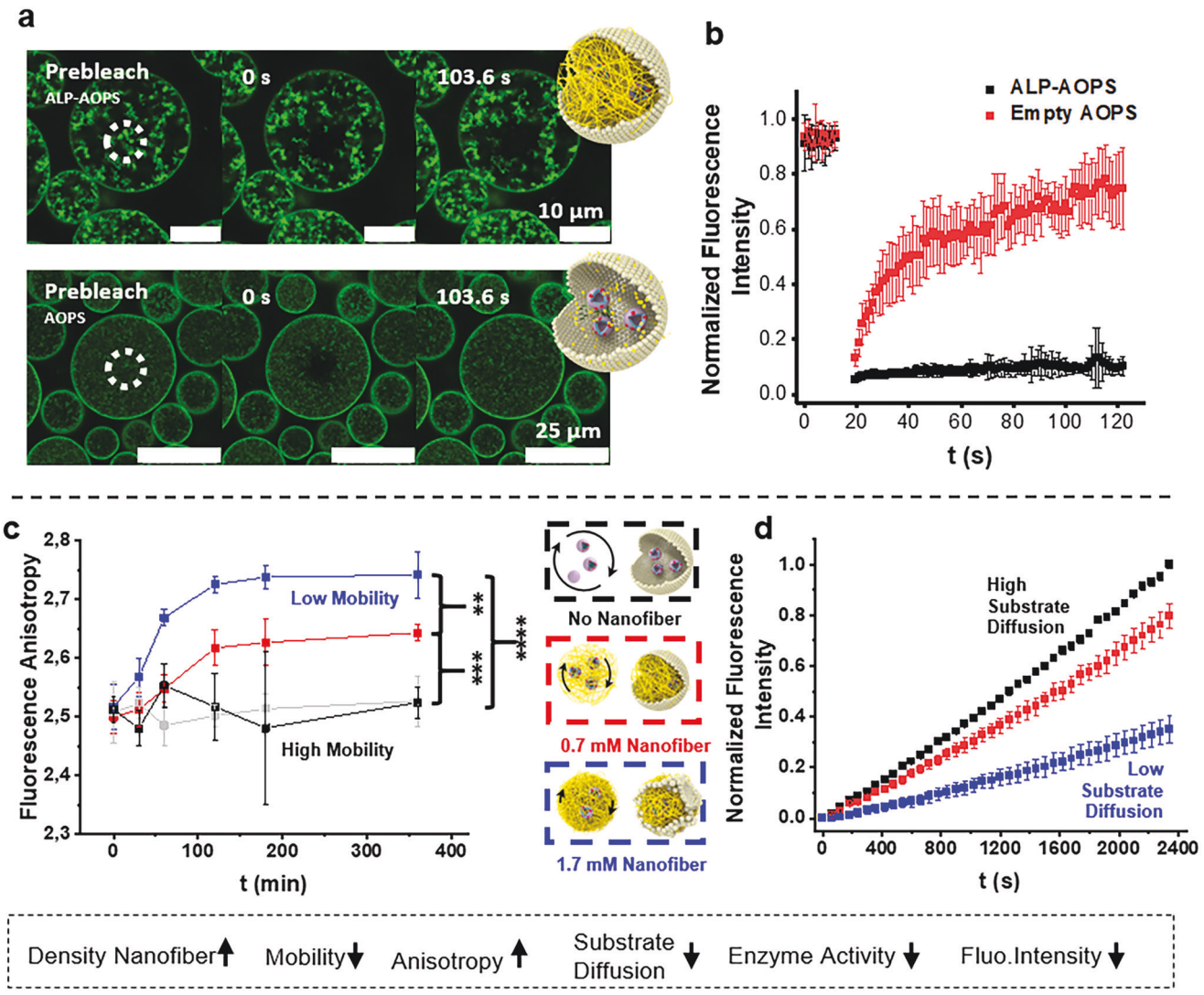

Figure 6. a,b) Dynamics and viscosity-like characterization of nanofiber within ALP-AOPS. FRAP study: Confocal fluorescence microscopy images of a representative ALP-AOPS (a-top) and empty AOPS (a-bottom) in the presence of 0.7 mM precursors after 6 h incubation; b) corresponding FRAP recovery curves for ALP-AOPS and empty AOPS after precursor treatment. c) Time-dependent fluorescence anisotropy study: ALP-AOPS in the presence of precursors (blue curve: 1.7 mM, red curve: 0.7 mM) and empty AOPS in presence of precursors (grey curve: 1.7 mM, black curve: 0.7 mM, controls). d) Enzymatic reaction rates in ALP-AOPS (black with no precursor, red with 0.7 mM precursor, blue with 1.7 mM precursor), conversion of non-fluorescent FDP as substrates into fluorescein. Enzyme assay conditions in Supporting Information.[8]

multi-compartmentalized protocells. The intracellular construction of the cytoskeleton-like scaffold in protocells is driven by the electrostatic interactions between the developing artificial cytoskeleton and the intracellular AOs and the outer proteinaceous membrane of protocells and is proven to be a time- and concentration-dependent process at physiological (=cytosol-like) conditions.

Thus, the increasing artificial cytoskeleton growth leads to a significant reduction in the mobility of the membrane-active AOs due to their integration in the cytoskeleton-like scaffold. Noteworthy, the desired enzymatic activity of ALP in AOs is still given, proven by the FDP assay after the formation of nanofibers-based scaffold within protocells. However, the ALP activity is dependent on the nanofibril density. Proven crowdedness, increased viscosity, and reduced diffusion rate of FDP substrate in the intracellular environment of protocells with increased cytoskeleton-like scaffold density are also accompanied by morphological transformation processes. ALP-AOPS change from spherical-like shapes into irregular protocell shapes when the oligopeptide concentration with the resulting nanofiber formation reaches a sufficient value (≥1.2 mM). Moreover, the crosslinked proteinaceous membrane of AOs-based protocells provides a high robustness and membrane elasticity to sustain bending and contraction processes over time.

Finally, the formation of cytoskeleton-like scaffold induced by AOs in our protocells and its influence on processes in the intracellular environment follow the same rules (e.g., concentration- and time-dependent parameters, viscosity, and diffusion) as

© 2023 The Authors. Advanced Functional Materials published by Wiley-VCH GmbH

16163028, 0, Downloaded from https://onlinelibrary.wiley.com/doi/10.1002/adfm.202306904 by Brandeis University, Wiley Online Library on [24/10/2023]. See the Terms and Conditions (https://onlinelibrary.wiley.com/terms-and-conditions) on Wiley Online Library for rules of use; OA articles are governed by the applicable Creative Commons License

in their natural counterparts. The protocell platform, developed in this study, is suited to mimic some characteristics of eukaryotic cells such as membrane-active AOs, enzyme-induced non-covalently assembled cytoskeleton, and regulable cytoplasm and enzyme reaction, high fluidity/elasticity of crosslinked proteinaceous membrane, and high mechanical stability of proteinosome-based protocells. The high flexibility of protocells membrane offers the future integration of actin filament components to study dynamic self-assembly and disassembly scaffold processes accompanied with morphological transformation processes for long-term use. It is expected that this artificial protocell holds great potential in synthetic biology and systems biology and may open new avenues for advancing eukaryotic cell mimicry with autonomous and self-regulating basic structures and functionalities.

4. Experimental Section

The synthetic protocols for block copolymers (BCPs) and BSA-PNIPAAm bioconjugates, as well as the fabrication methods for Empty-Psomes, ALP-Psomes, proteinosomes and AOPS, are available in detail in the Supporting Information.

Characterization of Nanofiber Formation in Bulk—Determination of Minimal Concentration of Precursors for Nanofiber Formation: 50 µL of purified ALP-Psomes (C_{BCP}: 0.5 mg mL^{-1}, in 10 mM PBS, pH 7.4) were mixed with 50 µL of precursors Nap-FFK(NBD)pY (0.112, 0.28, 0.56, 1.12, 2.24 mM, in 10 mM PBS, pH 7.4). After 3 h incubation at room temperature, 5 µL of samples were taken for TEM investigation (Figure S9, Supporting Information).

Characterization of Nanofiber Formation in Bulk—DLS Study: The size distribution of ALP-Psomes (C_{BCP}: 0.5 mg mL^{-1}) after the addition of non-labelled precursors (0.7 mM) in 10 mM PBS were monitored by DLS overtime, and Empty-Psomes (C_{BCP}: 0.5 mg mL^{-1}) sample treated with precursors was set as a control (Figure 1a,b; Table S2, Supporting Information).

Characterization of Nanofiber Formation in Bulk—Optical Density Measurements: The optical density of ALP-Psomes (C_{BCP}: 0.5 mg mL^{-1}) after the addition of non-labelled precursors (0.7 mM) in 10 mM PBS was monitored by UV–vis spectroscopy at 600 nm overtime, and Empty-Psomes (C_{BCP}: 0.5 mg mL^{-1}) sample treated with precursors was set as a control (Figure 1c).

Characterization of Nanofiber Formation in Bulk—CLSM Study: ALP-Psomes (C_{BCP}: 0.5 mg mL^{-1}) after the addition of precursors (0.7 mM) in 10 mM PBS were visualized by CLSM overtime, and Empty-Psomes (C_{BCP}: 0.5 mg mL^{-1}) sample treated with precursors was set as a control (Figure 1f, Figure S10, Supporting Information).

Characterization of Nanofiber Formation in Bulk—TEM Study: 50 µL of purified ALP-Psomes (C_{BCP}: 0.5 mg mL^{-1}, in 10 mM PBS, pH 7.4) were mixed with 50 µL of precursors Nap-FFKpY (2.24 mM, in 10 mM PBS, pH 7.4). 5 µL of samples were taken at the selected time points (30 min, 3 h, and 6 h) for TEM investigation. The same study was carried out to Empty-Psomes as control (Figure 1g; Figure S11, Supporting Information).

Characterization of Nanofiber Formation in ALP-AOPS—CLSM Study: 50 µL of ALP-AOPS (in 10 mM PBS, pH 7.4) were mixed with 50 µL of precursors Nap-FFK(NBD)pY (in 10 mM PBS, pH 7.4). Then, 15 µL of samples were pipetted into the sample holder and visualized by CLSM at selected time points (Figure 3a,b).

Characterization of Nanofiber Formation in ALP-AOPS—TEM Study: 50 µL of ALP-AOPS (in 10 mM PBS, pH 7.4) were mixed with 50 µL of precursors Nap-FFKpY (in 10 mM PBS, pH 7.4). 5 µL of samples were taken at each of the selected time points (30 min, 3 h, 6 h) for TEM investigation. The same study was carried out to Empty-AOPS as control (Figure 3c–f; Figure S14, Supporting Information).

Enzymatic Activity in ALP-AOPS in the Presence of Nanofiber—Comparison of Activity of ALP in the Presence of Various Densities of Nanofiber: 50 µL of ALP-AOPS (in 10 mM PBS, pH 7.4) were mixed with selected volumes (0, 10.6, 21.4, 41 µL) of precursor Nap-FFKpY (4 mM, in 10 mM PBS, pH 7.4), respectively, and the final volume was fixed to 100 µL. After 6 h incubation at room temperature, 10 µL of samples were taken and mixed with 5 µL of FDP (10 µM), followed by monitoring the changes in fluorescence intensity by a microplate reader (384-well plate, ex/em: 470 nm/515 nm).

Enzymatic Activity in ALP-AOPS in the Presence of Nanofiber—Comparison of Activity of ALP at Various pHs: 50 µL of ALP-AOPS (in 10 mM PBS, pH 7.4) were mixed with 21.4 µL of precursor Nap-FFKpY (4 mM, in 10 mM PBS, pH 7.4) and 28.6 µL of PBS buffer. After 6 h incubation, 30 µL of samples were taken and pH was adjusted to 6.0, 6.5, and 7.4 with HCl, respectively. Then, 15 µL of FDP (10 µM) were added. Afterward, the changes in fluorescence intensity were monitored by microplate reader (384-well plate, ex/em: 470 nm/515 nm).

Supporting Information

Supporting Information is available from the Wiley Online Library or from the author.

Acknowledgements

The authors express their gratitude for the opportunity to conduct this study within the Dresden International Graduate School for Biomedicine and Bioengineering (DIGS-BB). Special thanks are extended to Dr. Yixuan Du for providing valuable technical guidance in conducting TEM measurements, Alissa Seifert for conducting GPC measurements, and Dr. Hartmut Komber for performing NMR measurements. B.X. acknowledges the support of NIH CA142746 and NSF DMR-2011846. The Chair of Botany (C. Neinhuis) at the faculty of Biology of TU Dresden, Germany, is acknowledged for providing equipment and access to cryo-SEM.

Open access funding enabled and organized by Projekt DEAL.

Conflict of Interest

The authors declare no conflict of interest.

Author Contributions

D.W. conducted the majority of experiments and data analysis, and wrote the initial draft of the manuscript. S.M. contributed to project discussions, data analysis, and manuscript revision. M.G. participated in microscopic investigations, project discussions, and manuscript revisions. J.G. and B.X. provided the oligopeptides and guided the experiments for the self-assembly of oligopeptides into nanofibers. D.V. conducted cryo-SEM imaging of nanofiber-filled and non-filled proteinosomes. B.V. was responsible for project administration and manuscript revisions. D.A. provided the initial idea, supervised the project, and contributed to manuscript revisions.

Data Availability Statement

The data that support the findings of this study are available in the supplementary material of this article.

Keywords

artificial organelles, cytoskeleton, oligopeptides, polymersomes, protocells

Received: June 18, 2023
Revised: August 4, 2023
Published online:

© 2023 The Authors. Advanced Functional Materials published by Wiley-VCH GmbH

16163028, 0, Downloaded from https://onlinelibrary.wiley.com/doi/10.1002/adfm.202306904 by Brandeis University, Wiley Online Library on [24/10/2023]. See the Terms and Conditions (https://onlinelibrary.wiley.com/terms-and-conditions) on Wiley Online Library for rules of use; OA articles are governed by the applicable Creative Commons License

[1] T. Trantidou, M. Friddin, Y. Elani, N. J. Brooks, R. V. Law, J. M. Seddon, O. Ces, *ACS Nano* **2017**, *11*, 6549.
[2] K. Göpfrich, I. Platzman, J. P. Spatz, *Trends Biotechnol.* **2018**, *36*, 938.
[3] H. Jia, P. Schwille, *Curr. Opin. Biotechnol.* **2019**, *60*, 179.
[4] B. C. Buddingh', J. C. M. van Hest, *Acc. Chem. Res.* **2017**, *50*, 769.
[5] L. Schoonen, J. C. M. van Hest, *Adv. Mater.* **2016**, *28*, 1109.
[6] N. A. Yewdall, A. F. Mason, J. C. M. van Hest, *Interface Focus* **2018**, *8*, 20180023.
[7] A. F. Mason, N. A. Yewdall, P. L. W. Welzen, J. Shao, M. van Stevendaal, J. C. M. van Hest, D. S. Williams, L. K. E. A. Abdelmohsen, *ACS Cent. Sci.* **2019**, *5*, 1360.
[8] D. Wang, S. Moreno, S. Boye, B. Voit, D. Appelhans, *Chem. Commun.* **2021**, *57*, 8019.
[9] P. Wen, X. Wang, S. Moreno, S. Boye, D. Voigt, B. Voit, X. Huang, D. Appelhans, *Small* **2021**, *17*, 2005749.
[10] R. Booth, Y. Qiao, M. Li, S. Mann, *Angew. Chem., Int. Ed.* **2019**, *58*, 9120.
[11] J. Li, Z. Xu, M. Zhu, C. Zhao, X. Wang, H. Chen, X. Liu, L. Wang, X. Huang, *Chem* **2022**, *8*, 784.
[12] J. Li, M. Zhu, S. Wang, Z. Tao, X. Liu, X. Huang, *Chem. Commun.* **2021**, *57*, 11713.
[13] N.-N. Deng, W. T. S. Huck, *Angew. Chem.* **2017**, *129*, 9868.
[14] M. G. F. Last, S. Deshpande, C. Dekker, *ACS Nano* **2020**, *14*, 4487.
[15] C. Love, J. Steinkühler, D. T. Gonzales, N. Yandrapalli, T. Robinson, R. Dimova, T.-Y. D. Tang, *Angew. Chem.* **2020**, *132*, 6006.
[16] R. J. R. W. Peters, M. Marguet, S. Marais, M. W. Fraaije, J. C. M. van Hest, S. Lecommandoux, *Angew. Chem., Int. Ed.* **2014**, *53*, 146.
[17] M. Marguet, L. Edembe, S. Lecommandoux, *Angew. Chem., Int. Ed.* **2012**, *51*, 1173.
[18] S. Berhanu, T. Ueda, Y. Kuruma, *Nat. Commun.* **2019**, *10*, 1325.
[19] Z. Chen, J. Wang, W. Sun, E. Archibong, A. R. Kahkoska, X. Zhang, Y. Lu, F. S. Ligler, J. B. Buse, Z. Gu, *Nat. Chem. Biol.* **2018**, *14*, 86.
[20] Z. Feng, H. Wang, F. Wang, Y. Oh, C. Berciu, Q. Cui, E. H. Egelman, B. Xu, *Cell Rep. Phys. Sci.* **2020**, *1*, 100085.
[21] D. A. Fletcher, R. D. Mullins, *Nature* **2010**, *463*, 485.
[22] L. Blanchoin, R. Boujemaa-Paterski, C. Sykes, J. Plastino, *Physiol. Rev.* **2014**, *94*, 235.
[23] C. Kurokawa, K. Fujiwara, M. Morita, I. Kawamata, Y. Kawagishi, A. Sakai, Y. Murayama, S. M. Nomura, S. Murata, M. Takinoue, M. Yanagisawa, *Proc. Natl. Acad. Sci. U. S. A.* **2017**, *114*, 7228.
[24] X. Huang, A. J. Patil, M. Li, S. Mann, *J. Am. Chem. Soc.* **2014**, *136*, 9225.
[25] P. Zhan, K. Jahnke, N. Liu, K. Göpfrich, *Nat. Chem.* **2022**, *14*, 958.
[26] K. Jahnke, V. Huth, U. Mersdorf, N. Liu, K. Göpfrich, *ACS Nano* **2022**, *16*, 7233.
[27] Y. Bashirzadeh, N. H. Wubshet, A. P. Liu, *Front. Mol. Biosci.* **2020**, *7*, 610277.
[28] R. Kusters, C. Simon, R. L. D. Santos, V. Caorsi, S. Wu, J.-F. Joanny, P. Sens, C. Sykes, *Soft Matter* **2019**, *15*, 9647.
[29] E. Loiseau, J. A. M. Schneider, F. C. Keber, C. Pelzl, G. Massiera, G. Salbreux, A. R. Bausch, *Sci. Adv.* **2016**, *2*, e1500465.
[30] Y. T. Maeda, T. Nakadai, J. Shin, K. Uryu, V. Noireaux, A. Libchaber, *ACS Synth. Biol.* **2012**, *1*, 53.
[31] R. K. Kumar, M. Li, S. N. Olof, A. J. Patil, S. Mann, *Small* **2013**, *9*, 357.
[32] K. Akkarachaneeyakorn, M. Li, S. A. Davis, S. Mann, *Langmuir* **2016**, *32*, 2912.
[33] M. Marguet, C. Bonduelle, S. Lecommandoux, *Chem. Soc. Rev.* **2012**, *42*, 512.
[34] S. Yang, L. Jiang, *Chem. Commun.* **2020**, *56*, 8342.
[35] A. M. Brizard, J. H. van Esch, *Soft Matter* **2009**, *5*, 1320.
[36] R. Martí-Centelles, J. Rubio-Magnieto, B. Escuder, *Chem. Commun.* **2020**, *56*, 14487.
[37] H.-K. Lee, S. Soukasene, H. Jiang, S. Zhang, W. Feng, S. I. Stupp, *Soft Matter* **2008**, *4*, 962.
[38] O. Stauch, T. Uhlmann, M. Fröhlich, R. Thomann, M. El-Badry, Y.-K. Kim, R. Schubert, *Biomacromolecules* **2002**, *3*, 324.
[39] C. Campillo, B. Pépin-Donat, A. Viallat, *Soft Matter* **2007**, *3*, 1421.
[40] A. Brizard, M. Stuart, K. van Bommel, A. Friggeri, M. de Jong, J. van Esch, *Angew. Chem.* **2008**, *120*, 2093.
[41] A. Jesorka, M. Markström, M. Karlsson, O. Orwar, *J. Phys. Chem. B* **2005**, *109*, 14759.
[42] R. Krishna Kumar, X. Yu, A. J. Patil, M. Li, S. Mann, *Angew. Chem., Int. Ed.* **2011**, *50*, 9343.
[43] M. Dergham, S. Lin, J. Geng, *Angew. Chem., Int. Ed.* **2022**, *61*, e202114267.
[44] H. Wang, Z. Feng, B. Xu, *Chem. Soc. Rev.* **2017**, *46*, 2421.
[45] Z. Yang, G. Liang, B. Xu, *Acc. Chem. Res.* **2008**, *41*, 315.
[46] J. Dash, A. J. Patil, R. N. Das, F. L. Dowdall, S. Mann, *Soft Matter* **2011**, *7*, 8120.
[47] Y. Gao, J. Shi, D. Yuan, B. Xu, *Nat. Commun.* **2012**, *3*, 1033.
[48] Y. Kuang, J. Shi, J. Li, D. Yuan, K. A. Alberti, Q. Xu, B. Xu, *Angew. Chem.* **2014**, *126*, 8242.
[49] Z. Feng, H. Wang, R. Zhou, J. Li, B. Xu, *J. Am. Chem. Soc.* **2017**, *139*, 3950.
[50] H. Wang, Z. Feng, B. Xu, *J. Am. Chem. Soc.* **2019**, *141*, 7271.
[51] S. Moreno, P. Sharan, J. Engelke, H. Gumz, S. Boye, U. Oertel, P. Wang, S. Banerjee, R. Klajn, B. Voit, A. Lederer, D. Appelhans, *Small* **2020**, *16*, 2002135.
[52] K. Zhang, S. Moreno, X. Wang, Y. Zhou, S. Boye, D. Voigt, B. Voit, D. Appelhans, *Biomacromolecules* **2023**, *24*, 2489.
[53] P. Wang, S. Moreno, A. Janke, S. Boye, D. Wang, S. Schwarz, B. Voit, D. Appelhans, *Biomacromolecules* **2022**, *23*, 3648.
[54] X. Wang, S. Moreno, S. Boye, P. Wen, K. Zhang, P. Formanek, A. Lederer, B. Voit, D. Appelhans, *Chem. Mater.* **2021**, *33*, 6692.
[55] J. Li, Y. Gao, Y. Kuang, J. Shi, X. Du, J. Zhou, H. Wang, Z. Yang, B. Xu, *J. Am. Chem. Soc.* **2013**, *135*, 9907.
[56] E. Rideau, R. Dimova, P. Schwille, F. R. Wurm, K. Landfester, *Chem. Soc. Rev.* **2018**, *47*, 8572.
[57] W.-S. Jang, S. C. Park, E. H. Reed, K. P. Dooley, S. F. Wheeler, D. Lee, D. A. Hammer, *Soft Matter* **2016**, *12*, 1014.
[58] A. Peyret, E. Ibarboure, A. Tron, L. Beauté, R. Rust, O. Sandre, N. D. McClenaghan, S. Lecommandoux, *Angew. Chem., Int. Ed.* **2017**, *56*, 1566.
[59] X. Huang, M. Li, D. C. Green, D. S. Williams, A. J. Patil, S. Mann, *Nat. Commun.* **2013**, *4*, 2239.
[60] J. Zhou, X. Du, C. Berciu, H. He, J. Shi, D. Nicastro, B. Xu, *Chem* **2016**, *1*, 246.
[61] L. Sixdenier, A. Auge, Y. Zhao, E. Marie, C. Tribet, *ACS Macro Lett.* **2022**, *11*, 651.

© 2023 The Authors. Advanced Functional Materials published by Wiley-VCH GmbH

16163028, 0, Downloaded from https://onlinelibrary.wiley.com/doi/10.1002/adfm.202306904 by Brandeis University, Wiley Online Library on [24/10/2023]. See the Terms and Conditions (https://onlinelibrary.wiley.com/terms-and-conditions) on Wiley Online Library for rules of use; OA articles are governed by the applicable Creative Commons License